Elastomechanical and Magneto-Optoelectronic Investigation of $RbCoF_3$: An *ab initio* DFT Study

N. Erum[a,*] and M.A. Iqbal[b]

[a] *Physics Department, The University of Lahore, Defence Road, Lahore, Pakistan*
[b] *School of Science, University of Management and Technology, C-ll Johar Town Campus, Lahore, Pakistan*

Received: 19.03.2020 & Accepted: 15.05.2020

Doi: 10.12693/APhysPolA.138.509 *e-mail: erum.n@hotmail.com

In this study, within the framework of density functional theory by using full potential linearized augmented plane wave method comprehensive *ab initio* calculations are done, in order to investigate structural, elastic, mechanical, and magneto-optoelectronic aspects of $RbCoF_3$ fluoro-perovskite. Investigated structural properties by analytical methods as well as density functional theory establish to be similar in comparison with results of experimental data. The elastic and mechanical properties confirmed that $RbCoF_3$ is elastically stable, as well as anisotropic. Furthermore, by calculating the Debye temperature θ_D, thermal behavior of the compound is explored. However, spin dependent magneto-electronic parameters expose that exchange splitting is ruled by Co 3*d* orbital. The optimizations of stable magnetic phase authenticates the low temperature experimental observations. The optical spectra also deliver various linear optical parameters. Therefore, the current investigation signifies a valuable approach to analyze the comprehensive data about structural magneto-electronic and optical properties that can create a prospect to comprehend profuse physical occurrences, in addition to this, authorize material scientists to implement this materials for spintronic applications.

topics: fluoro-perovskites, first-principles study, magneto-electronic property, optical property

1. Introduction

Half-metallic compounds are worthy to mention in order to attain progressive technological needs. They are classified as useful economically efficient compounds. At about the Fermi level, they have the ability to maintain merely one spin direction. In perovskite materials, the investigation of half-metallic are generally associated with their possible applications in the field of magnetoresistive memories, magnetoresistive sensors, in addition to it spin based devices, e.g. magnetic storage systems, as well as spin valve [1–6].

The general formula for complex fluoride perovskite is ABF_3 where cations are A and B, though F is fluorine monovalent anion. In this $RbCoF_3$, rubidium based fluoride perovskite is a theme of various distinctive aspects, like phenomenon of half-metallicity, high temperature superconductivity, colossal magnetoresistivity, ferroelectricity, phase separation, semiconductivity, piezoelectricity, thermoelectricity, catalytic activity, photoluminescence, and phenomenon of metal–insulator transition. To improve tunneling magnetoresistance (TMR) in magnetic tunnel junctions (MTJs), this class of materials have gained huge interest in various areas of spintronics. In actual the mechanism of spintronic depends upon the charge of electrons accompanied by its spin, that can deliver gigabit memory devices [7, 8].

Generally, $K/RbCoF_3$ crystals crystallizes themselves in ideal structure of cubic perovskite that have been experimentally confirmed by Lee et al. [9] and Manivannan et al. [10]. Ito and Narita [11] applied the Mössbauer spectroscopy to $KFeF_3$ samples between 4.2 K and 300 K. Thin single crystal slices were stressed along the respective plane that used to determine the orientation of the hyperfine field (H_{hf}) and the principal axes of the electric field gradient (EFG) tensors. In fact, H_{hf} and z are parallel to the [111] direction between $T_N = 112$ K and ≈ 65 K (where T_N is the Néel temperature). Below ≈ 65 K a rotation of the principal axes of the EFG tensors takes place. Below $T_C = 41$ K (where T_C is the Curie temperature) H_{hf} is still parallel to the [111] direction within 5° but the principal axis x of the EFG tensors lies in the (110) plane and makes an angle θ (40° at 4.2 K) to the [111] direction. The weak ferromagnetic moment parallel to the $\langle 110 \rangle$ direction was observed below T_C. Shafer [12] investigates unique ferrimagnetic configurations in $RbMgF_3$–$RbCoF_3$ system where Co^{2+} is the only magnetic transition metal ion. Punkkinen [13], theoretically, explores phenomenon of *d*-states correlation in potassium based perovskites $KFeF_3$ and $KCoF_3$. It can be inferred from previous work that $RbCoF_3$ compounds possess advantageous magneto-optoelectronic aspects.

This research based manuscript will dedicate to contribute under cover magneto-optoelectronic plus

TABLE I

Comparison of experimental and calculated values of equilibrium lattice constants a_0, bulk modulus B_0 and its pressure derivative B_P, and bond lengths of $RbCoF_3$ compounds.

	This work				Other works	
	GGA	LSDA	IR method (analytical)	VJ method (analytical)	Experimental	Theoretical
a_0 [Å]	4.151	4.143	4.159	3.989	4.141 [23]	4.143 [24], 4.141 [25] 4.140 [26], 4.117 [26], 4.108 [23], 3.884 [27]
B_0 [GPa]	70.12	70.15				71.45 [28]
B_P [GPa]	5.15	5.18				
Bond-lengths						
Rb–F [Å]	2.98					
Rb–Co [Å]	3.54					
Co–F [Å]	2.04				2.06 [29]	

thermal aspects of corresponding ternary fluorides. Consequently, because of inadequate earlier studies, the following compound requires additional explorations, that encourage us to investigate it in detail. In order to describe important outcomes, we inspect ground state electronic structure, mechanical, magnetic, thermal, as well as optical properties of $RbCoF_3$ fluoro-perovskite. In order to accomplish ultimate scientific applications, the manuscript is organized as follows: Opening section is devoted to explore few of fundamental aspects of materials as well as their associated applications. Subsequent section explains computational method for calculated work, whereas third section represents detailed results plus potential considerations for numerous aspects, and where data available, it is compared with preceding studies. Lastly conclusion is attained to clarify upcoming prospective of the research.

2. Method of calculation

To calculate spin-polarized structural, elastic, electronic and magneto-optic properties of rubidium based fluoro-perovskite $RbCoF_3$, the full potential linearized augmented plane wave (FP-LAPW) method is applied to elucidate the Kohn–Sham equations [14] derived in density functional theory (DFT) [15–17], by means of different exchange correlation approximation like local spin density approximation (LSDA) [18], generalized gradient approximation (GGA) [19], as well as recently bugged GGA plus trans-Blaha modified Becke–Johnson (TB-mBJ) potential [20]. Additionally, optimizations of each unit cell are performed to obtain ground state structural parameters by fitting Birch–Murnaghan equation of state [21]. Moreover, cubic-elastic software is used to calculate the elastic constants of $RbCoF_3$ fluoro-perovskite. Comprehensive explanation of cubic-elastic software are presented in [22]. The details of spin-dependent

TABLE II

Mechanical properties obtained for $RbCoF_3$ compounds.

Parameter	Value	Parameter	Value
C_{11} [GPa]	113.85 (122.282 [30])	C_{12} [GPa]	47.126 (52.919 [30])
C_{44} [GPa]	24.597	B_0 [GPa]	69.363
G_{V} [GPa]	28.104	G_{R} [GPa]	27.486
G_{H} [GPa]	27.795	B_0/G_{H} [GPa]	2.495
C'	33.36	C''	22.61
Y [GPa]	73.559	v [GPa]	0.32
A [GPa]	0.75	ξ [GPa]	0.55
λ	49.52	μ	27.85

FP-LAPW method, its computational information regarding WIEN2K package, used in this work can be found in [23]. In WIEN2K package, valence electrons treatment are done semirelativistically, although core electrons are treated fully relativistically. However, for convergence in basis size, a cut-off value of $R_{\mathrm{MT}}K_{\max} = 8.0$ is used. Additionally, to achieve well-converged optimum results of structural properties, 56 K point integration in the Brillouin zone (BZ) is done with modified form of tetrahedron method. Conversely, for calculating electronic, as well as magneto-optic properties a denser mesh of 2000 K-points are used. The self-consistence calculations are considered to be converged when the convergence tolerance of energy and charge are less than 0.00001 Ry and 0.0001 electron charges, respectively. According to Table I and Table II, the bulk modulus values are calculated by two ways, one by fitting volume versus energy curve and another by using elastic constant formula as mentioned in [31]. All calculated properties are done by considering ferromagnetic (FM) ordering.

3. Results and discussion

3.1. Structural properties

$RbCoF_3$ crystallizes in cubic structure, in which the Wyckoff coordinates occupy 1a (000), 1b $(0.5, 0.5, 0.5)$, and 3c $(0, 0.5, 0.5)$ for Rb, Co, and F, correspondingly. Figure 1 illustrates the total energy as a function of unit cell volume in which the ground state energies are determined by using Birch–Murnaghan's equation of state (EOS) [21]. The resultant ground state spin-polarized structural properties at $T = 0$ K for $RbCoF_3$ fluoro-perovskite for example, ground state lattice constant a_0, optimized energy E_0, bulk modulus and their pressure derivative, B_0 and B_P respectively, by local spin density approximation (LSDA) and generalized gradient approximation (GGA) exchange correlation schemes are presented in Table I. These values agree well with available experimental [23, 29] and previous theoretical results [24–28]. The lattice constants of $RbCoF_3$ fluoro-perovskites are also calculated analytically by two methods. Prior is ionic radii method, while Verma and Jindal predict the prior method. The former method utilizes formula such as [30, 32]:

$$a_0 = \alpha + \beta\left(r_{\mathrm{Rb}} + r_{\mathrm{F}}\right) + \gamma\left(r_{\mathrm{Co}} + r_{\mathrm{F}}\right), \tag{1}$$

where $\alpha = 0.06741$, $\beta = 0.4905$, $\gamma = 1.2921$ are the constants, while the ionic radii for given species are given accordingly $r_{\mathrm{Rb}} = 1.72$Å, $r_{\mathrm{Co}} = 0.75$Å, and $r_{\mathrm{F}} = 1.33$Å [33]. Verma and Jindal suggest that lattice constant calculation based upon valence electrons, as well as ionic radii should use subsequent relation [34]:

$$a_0 = K r_{\mathrm{avg}} \left(V_{\mathrm{Rb}} V_{\mathrm{Co}} V_{\mathrm{F}}\right)^S, \tag{2}$$

where V_{Rb}, V_{Rb}, and V_{F} are the numbers of valence electrons in Rb, Co, and F, respectively, and r_{avg} denotes average ionic radii of $RbCoF_3$ compounds. For cubic system, $K = 2.45$ and $S = 0.09$. The resultant lattice constants values obtained with (1) and (2) are shown in Table I. One can observe that there is reasonable discrepancy between DFT calculated lattice constants as compared to the analytical one. The source of this divergence might be not trivial, e.g., in the calculation, we took the data (the ionic radii and valence electrons of the individual atoms) from [33] and, e.g., the lower accuracy of the constants (α, β and γ) in (1) and K and S in (2). In addition, the calculated lattice constants are predicted at $T = 0$ K. Nevertheless, DFTs versus experimental results are suitably consistent with each other.

Table I also demonstrates chemical nature with the aid of chemical bonding, which can further explore structural symmetry with regard to tolerance factor. The tolerance factors as shown in Table III are calculated using the following formula [35]:

$$t = \frac{0.707\langle \mathrm{Rb} - \mathrm{F}\rangle}{\langle \mathrm{Co} - \mathrm{F}\rangle}, \tag{3}$$

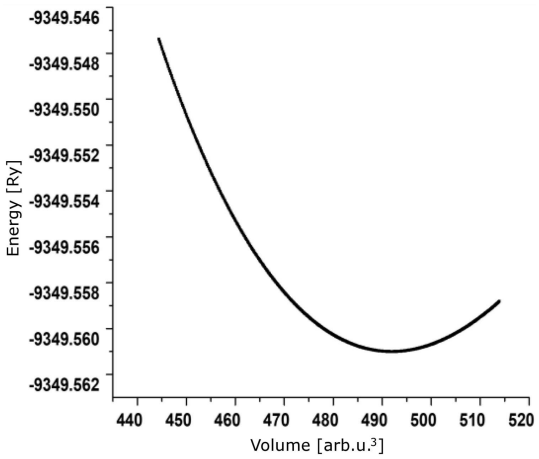

Fig. 1. Variation of total energy E (Ry) as a function of unit cell volume V [a.u]^3 for $RbCoF_3$.

TABLE III

Tolerance factor calculated for $RbCoF_3$ compound.

Bond length formula	Goldschmidt's formula	Ref. [23]
1.032	1.046	1.047

where $\langle$Rb–F$\rangle$ and $\langle$Co–F$\rangle$ is the average bonds length between Rb, Co, and F, respectively. In general, the allowed range of tolerance for cubic perovskite compound lies between 0.95 and 1.04 [36]. In this way, the compound satisfies reliability of the investigated calculations by fulfilling good tolerance factor criteria for cubic perovskites.

3.2. Elastic properties

With elastic constants of solids we can be able to provide valuable parameters regarding to the structural stability and the useful binding characteristic [37–39]. There are three independent elastic constants denoted by C_{11}, C_{12} and C_{44} for cubic system which are listed in Table II. These compounds fulfill traditional mechanical stability condition at $P = 0$ GPa and also satisfy cubic stability condition, i.e., $C_{12} < B < C_{11}$ which indicates the general elastic stability and cubic phase elastic stability, respectively [40]. For $RbCoF_3$, the value of elastic constant C_{11} is higher than C_{12} as well as C_{44}. These results reveal that $RbCoF_3$ hold more resistance to compression as compared to shear deformation, because the ratio of value of C_{11} is many times higher than that of C_{44}. Similar trends of C_{11} and C_{44} elastic constants are observed in [40] and [41], which agrees well with behavior of our compounds and other available results [30, 42]. In general, finite temperature tends to reduce the elastic constant values with the thermal expansion, which is also confirmed theoretically as well as experimentally for other fluoro-perovskites, for example $KMgF_3$, as well as $KZnF_3$, $CsCdF_3$ [43–45].

3.3. Mechanical properties

Here, our aim is to calculate mechanical properties, i.e., Voigt's modulus, Hill's modulus, Reuss's modulus, bulk modulus, shear modulus, Young's modulus, elastic stiffness coefficients, Lamé's coefficients, Poisson's ratio and Kleinman's parameter. Details of mathematical relationships can be found in [31, 46–49].

The value of both bulk and shear modulus are used to determine hardness of materials. The agreement between calculated bulk modulus from elastic constants and from the Birch–Murnaghan equation of state, can be observed in Table II. This confirms the highly accurate calculation of elastic constants. From the present results it can be observed that $RbCoF_3$ is class of stiffer material, which infers its high tendency of charge transfer among anion. Cauchy's pressure $(C_{12} - C_{44})$, Poisson's ratio (v), and Pugh's index of ductility (B/G) are the main factors that gives information either the material is ductile or brittle in nature [50]. Hence, $B/G > 1.75$ and Cauchy's pressure $C^{''} > 0$, and $v > 0.26$ for the rest of compounds imply that they are ductile and contain high directional bonding. These compounds have high shear constant's values, which approves its covalent nature. The elastic anisotropy parameter A is used to quantify extent of elastic anisotropy and the crystals can be completely classified as isotropic if the value of A is unity [51–54]. Based on results in Table II, it can be noticed that rubidium based fluoro-perovskite compound $RbCoF_3$ is characterized as highly anisotropic. The purpose of first Lamé's constant λ is to represent the compressibility of the material and the second Lamé's constant μ represents the (shear) stiffness which is in agreement with previous study of $RbNiF_3$ [54] and above mentioned findings.

3.4. Thermal properties (calculation of the Debye temperature)

The Debye cut-off frequency or the Debye temperature (θ_{D}) is a significant form of temperature, which was used to quantify several thermodynamic properties in the solid. It is important because it delivers some useful physical quantities, for example specific heat and melting point. There are two key methods to calculate the Debye temperature (θ_{D}), namely elastic constant method and from specific heat measurements. In this manuscript, we consider elastic constant method to calculate the Debye temperature (θ_{D}) and associated parameters following the formulae in [55]. The resultant quantities of our calculations such as the Debye temperature, average sound velocity, and melting point are presented in Table IV, which agrees well with previous theoretical results [54]. However, some deviation is observed from available experimental results because present calculations are carried out at 0 K while experimental results are taken at finite temperature. In fact, density of the compound is low at 0 K, which retains inverse relation with respect to the Debye temperature [59]. Furthermore, the difference in melting point is endorsed due to large error (±300 K) which is due to exchange-correlation potential, which can be able to cancel miscalculations between total energies of atoms with more homogeneous solids. However, it can be observed that calculated transverse and longitudinal sound velocities are higher for $RbCoF_3$, because the Debye temperature θ_{D} has direct relation with average sound velocity, and so highest value of the Debye temperature θ_{D}. Similar findings are observed for melting temperature. As far as we know, this is the first theoretical study on thermal properties of perovskite-type fluorides $RbCoF_3$ compounds. We hope that this investigation may motivate an insight associated to their performance in related fields.

TABLE IV

Comparison of experimental and calculated values for $RbCoF_3$.

	Present work	Experimental
ρ [g/cm^3]	5.18	4.76 [42]
υ_l [K m/s]	5.35	
υ_t [K m/s]	2.52	
υ_m [K m/s]	3.93	3.31 [56]
θ_{D} [K]	498	239 [57]
T_{melt} [K]	1225 ± 300	1148 [42], 1300 [58]

3.5. Magnetoelectronic properties

This subsection is dedicated to consider the magnetoelectronic properties of $RbCoF_3$ compounds. To illustrate the electronic properties spin dependent bandstructures are calculated by LSDA exchange and correlation scheme [18–20] as shown in Fig. 2a and 2b. The Fermi level is set at 0 eV. For $RbCoF_3$, the energy gap is absent for the spin down channel, thus indicating their metallic behavior in the spin-down channel. On the other hand, for spin up channel energy gaps is present as shown in Fig. 2a, so it can be concluded that $RbCoF_3$ compounds exhibit a half-metallic character, which is in reasonable agreement with the behavior of previous study [6, 10].

The density of states (DOS) structures occupy energy E_{F} intervals from -10 eV up to $+10$ eV as shown in Fig. 3. The extended band is observed at $E_{\mathrm{F}} = -5$ eV due to presence of F $2p$ states with small hybridization of Co d states. Next energy interval from $E_{\mathrm{F}} = -5$ eV to $E_{\mathrm{F}} = +5$ eV is mainly composed of d states of transition metals. The hybridization between Co and F states in the first and second regions of the valence band is obvious. This contribution can be attributed to the high attraction that occurs between the positive charges of Co with the negative charge of F in the octahedron CoF_6 structure. While above Fermi level, the conduction band is formed due to states of Rb: $3d$ hybridized with Rb $3p$ and

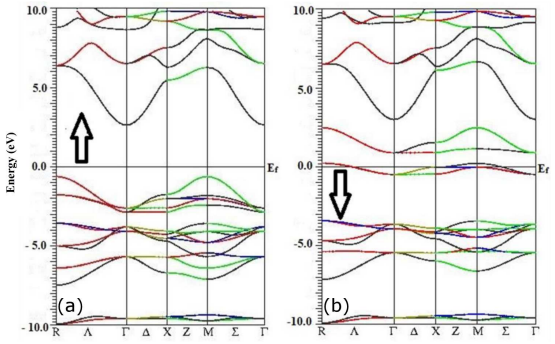

Fig. 2. Spin dependent electronic band structures of $RbCoF_3$ (a) LSDA (spin up) (b) LSDA (spin down).

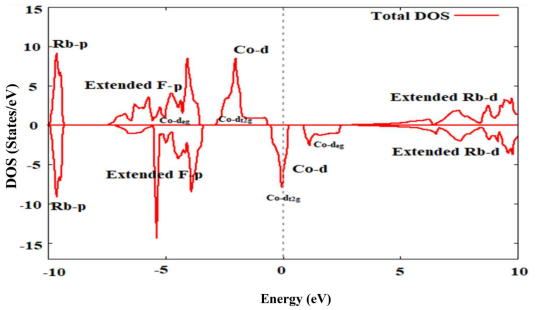

Fig. 3. Spin-dependent total and partial density of states for $RbCoF_3$.

Rb 3*s* states. As a whole crystal, fields are generated in general due to Coulomb's repulsion in between electronic states of Co 3*d* and F 2*p* states, which causes splitting of 3*d* states of transition metals into two non-degenerate states, namely t_{2g} and e_g [60]. Moreover, it is evident that in the spin down part of the total DOS, local and mostly no hybridized (Co)*d*–t_{2g} states are found above the Fermi level, which confirms their metallic behavior for the spin-down channel. The spin up channel has a band gap, resulting in 100% spin polarization of the charge carriers and this compound favorable for spintronics devices.

Charge density contours can be able to explore nature of bonding in crystalline solids [61] which are calculated along (110) planes for corresponding channels of spin up and spin down as displayed in Fig. 4. The density plots in (110) direction indicate that Co states are almost spherical for majority spin channel, which relates to that the transition metal 3*d* states are partially filled (see Fig. 2a, b). In detail bonding between Rb–F, ions are ionic, since very less overlapping is observed between Rb and F ions. However, in case of minority spin channel, the change in shape of Co states occurs approximately from spherical to dumbly, which illustrates ionic interaction with F 2*p* states. As a whole bonding between Co and F, ions are strongly covalent as large sharing is observed, because *pd*-hybridization among cations and anions depends on covalent nature.

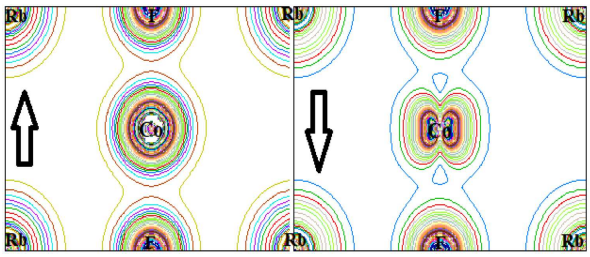

Fig. 4. Spin-dependent electron charge densities in (110) planes for $RbCoF_3$.

TABLE V

Comparison of calculated interstitial M^{inst}, local and total magnetic moment M^{T} of $RbCoF_3$ compound with available experimental [63] and other theoretical [30] data.

Magnetic moment	Value [μ_{B}]
M^{inst}	0.05134
M^{Rb}	−0.00077
M^{Co}	2.6782 (2.3 [30])
M^{F}	0.0713
M^{T}	3.00012 (3.12 [63])

The origin of magnetism is attributed to combination of discrete atoms according to crystalline structure of solids. The concept of magnetism exists due to partially filled electron shells [62]. To study magnetic behavior of $RbCoF_3$ compound we calculate total, interstitial and local magnetic moments as presented in Table V, which are in reasonable agreement with earlier theoretical plus available experimental data [30, 63, 64]. The spin magnetic moments of $RbCoF_3$ mostly originated from the transition metal element, leading to almost no contribution from the Rb and F sites. It can be seen that Rb and F have negligible magnetic moments, which suggests that the total magnetic moments are all contributed by the Co atoms. Half-metallic nature of $RbCoF_3$ can also be confirmed by integer value of the total magnetic moment which is in agreement with the Slater–Pauling rule [65], whereas negative signs demonstrate that Rb atoms are antiparallel to Co atoms in $RbCoF_3$, which consequently reduces the net magnitude of magnetic moments in this compound and the occurrence of these magnetic moments are due to orbital extended and total polarization. However, the positive magnetic moments of interstitial sites and F atoms reveal they are in actual parallel to magnetic moments of Co atoms. The variation in calculated magnetic moment is due to transfer of electron from partially filled transition metals to fluorine atoms. These prominent characteristics make these compounds suitable for application in spintronic based switching devices.

3.6. Optical properties

This section is devoted to explore the optical properties of $RbCoF_3$ compounds to the applied field of electromagnetic radiation with GGA approximation. The optical properties are calculated using complex form of dielectric function denoted as $\varepsilon(\omega)$ [66], namely

$$\varepsilon(\omega) = \varepsilon_1(\omega) + i\varepsilon_2(\omega). \quad (4)$$

These properties include the energy loss function $L(\omega)$, absorption coefficient $\alpha(\omega)$, optical conductivity $\sigma(\omega)$, refractive index $n(\omega)$, reflectivity $R(\omega)$, and the effective number of electrons (n_{eff}) by sum rules along x-direction are presented in Figs. 5–12, for the energy range up to 30 eV. Our analysis of corresponding ε_2 (ω) peaks trail the similar pattern of DOS and band structure of investigated compounds. The point of threshold energy occurs within 0–5 eV for $RbCoF_3$ compound, respectively. After that, till 20 eV, diversified peaks are observed. However, the major peaks are positioned at about 23 eV that corresponds to transition from occupied (Co d and F p) valence band states to unoccupied (Co d and Rb d) conduction band states.

In the spectrum of real part of dielectric function $\varepsilon_1(\omega)$, the zero frequency limit $\varepsilon_1(0)$ which provides static dielectric constant (see Fig. 6) in the zero frequency limits. It is located at about 2.12 eV

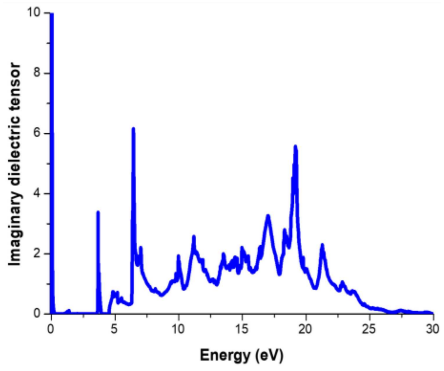

Fig. 5. Calculated imaginary part $\epsilon_2(\omega)$ of the dielectric function for $RbCoF_3$ compounds.

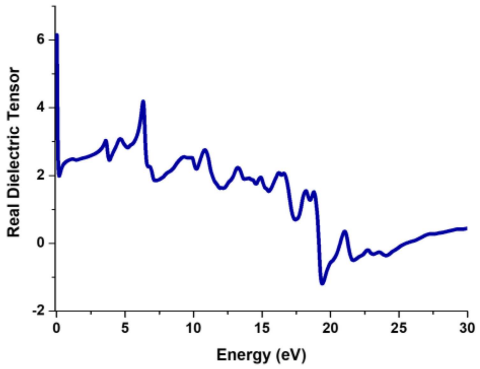

Fig. 6. Calculated real part $\epsilon_1(\omega)$ of the dielectric function for $RbCoF_3$ compounds.

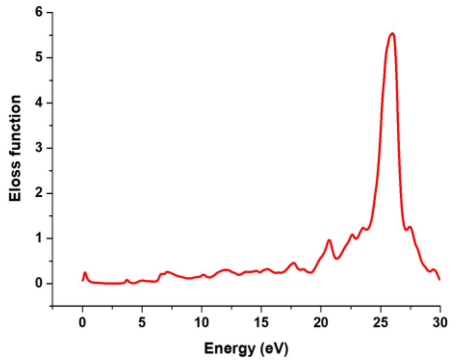

Fig. 7. Calculated energy loss function $L(\omega)$ of the dielectric function for $RbCoF_3$ compounds.

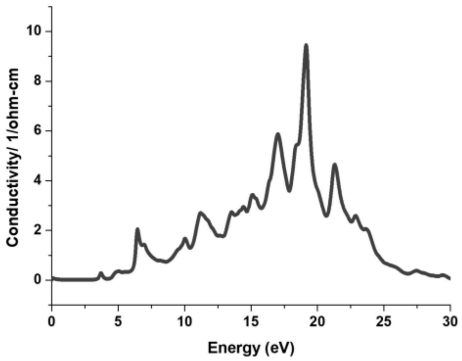

Fig. 8. Calculated conductivity $\sigma(\omega)$ of the dielectric function for $RbCoF_3$ compounds.

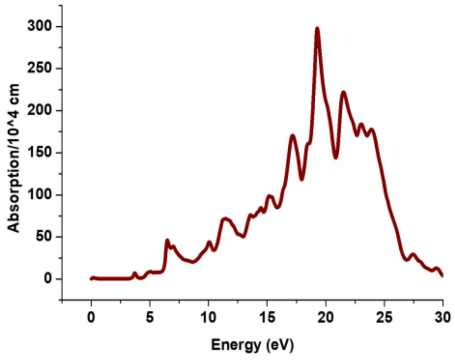

Fig. 9. Calculated absorption coefficient $\alpha(\omega)$ of the dielectric function for $RbCoF_3$ compounds.

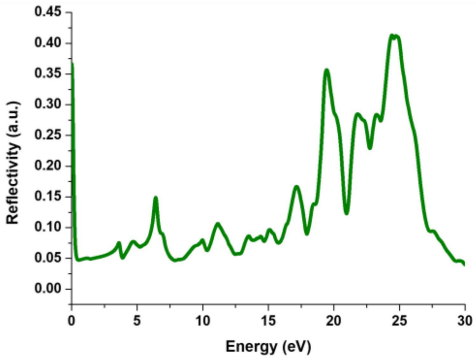

Fig. 10. Calculated reflectivity $R(\omega)$ of the dielectric function for $RbCoF_3$ compounds.

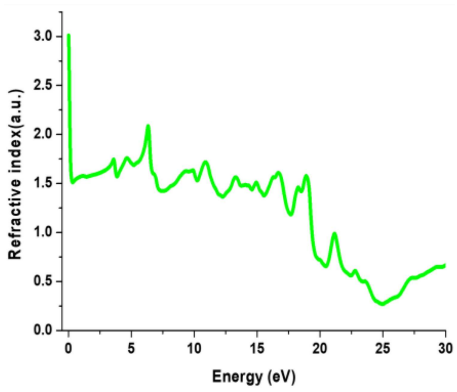

Fig. 11. Refractive index $n(\omega)$ of the dielectric function for $RbCoF_3$ compounds.

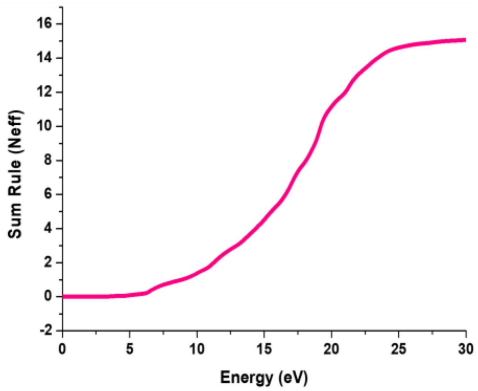

Fig. 12. Calculated sum rule N_{eff} of the dielectric function for $RbCoF_3$ compounds.

for $RbCoF_3$. The increasing curves of $\varepsilon_1(\omega)$ attains maximum value approximately at 6.42 eV. Then, the curves showed sudden decrease following fluctuation until reaching 18.87 eV. The minimum peaks are positioned approximately at 19 eV where propagation of photons are entirely attenuated within the optical limit.

The electron energy loss spectrum $L(\omega)$, illustrates distinctive Plasmon oscillations [67] as seen in Fig. 7. A sharp plasmon peak is seen at approximately 27.0 eV. These peaks can be associated to the trailing edge of the $R(\omega)$ (see Fig. 10). The purpose of optical conductivity $\sigma(\omega)$ is to describe the phenomenon of electron conduction due to applied electromagnetic field as shown in Fig. 8. The phenomenon of conductivity originates at about 5 eV from small ascending peak which finally reaches to its divergent sharp maxima at about 19 eV. From the plot of absorption coefficient it can be inferred that compounds initiate absorbing electromagnetic radiation at about value of 4.25 eV as displayed in Fig. 9. This particular energy (threshold point) is exactly in accordance with trend of band gaps and $\sigma(\omega)$ plots. However, these compounds start absorption within range of 19–23 eV and noticeable peak is detected at about 20 eV. After the advent of optimum absorption peaks spectrum again going to decrease suffering with the trivial variations. From the analysis of absorption spectra it can be concluded that in wide ultraviolet region, typically at about 20 eV some beneficial magneto-optoelectronic application of this fluoro-perovskites can be achieved. This behavior is in accordance with previously studied fluoro-perovskites [68, 69]. The calculated reflectivity spectrum $R(\omega)$ interprets optical transitions of a material as shown in Fig. 10. The reflection spectra begins reflecting highly and attains maximum value within 20–26 eV. Hence, these materials show transparency in this particular energy range. Therefore, these compounds can be utilized as protective agents from UV radiation.

The calculated refractive index $n(\omega)$ along x direction is shown in Fig. 11, which depicts material's transparency versus spectral radiation. The knowledge of refractive index plays an important role for the versatile application optoelectronic devices such as photonic crystals, solar cells, and detectors [61]. It can be observed that transition metal based fluoro-perovskites exhibit high refractive indices at low energies. The index of refraction attains a maximum value within energy range of UV-spectrum, which is due to excitonic transitions nearly at energy band-gap edge. However the static part of refractive index $n(0)$ is found to be approximately at 1.5. The oscillator strength as shown in Fig. 12 depicts inter-band transition of electrons in zero up to 5 eV. After that the trend-line increases slowly but there is advent of sharp peak presenting abrupt increase of electron which saturates in the range of about 23–26 eV.

4. Conclusions

In summary, all electron self-consistent FP-LAPW method is used to theoretically investigate $RbCoF_3$ fluoro-perovskite by various approximations based on DFT. Our calculations show that the DFT band-gap results are much consistent with the available experimental data. Structural properties are calculated by DFT as well as by analytical methods and are found in close agreement with each other. A complete description of elastic, mechanical, and some of thermal parameters confirms anisotropic and mixed covalent-ionic nature. The investigated magnetoelectronic behavior reveals dominancy of Co $3d$ orbital in exchange splitting while values of magnetic moments are found consistent with the low temperature experimental observations. Optical properties show that these compounds have wide range of absorption and reflection in high frequency regions. Consequently, through this investigation various magneto-optoelectronic effects has benchmarked, which should be considered in future for fabricating practical spintronic devices for their possible technological benefits.

References

[1] D. Zhang, S. W. Eaton, Y. Yu, L. Dou, P. Yang, *J. Am. Chem. Soc.* **137**, 9230 (2015).

[2] T. Leijtens, G.E. Eperon, N.K. Noel, S.N. Habisreutinger, A. Petrozza, H.J. Snaith, *Adv. Energy Mater.* **5**, 1500963 (2015).

[3] E.M. Erickson, C. Ghanty, D. Aurbach, *J. Phys. Chem. Lett.* **5**, 3313 (2014).

[4] Z. Ali, A. Sattar, S.J. Asadabadi, I. Ahmad, *J. Phys. Chem. Solids* **86**, 114 (2015).

[5] R.V. Pisarev, I.G. Siny, G.A. Smolensky, *Solid State Commun.* **7**, 23 (1969).

[6] R. Narayan, S. Ramaseshan, *J. Phys. Chem. Solids* **39**, 1287 (1978).

[7] H. Ohno, A. Sher, F. Matsuka, A. Oiwa, A. Eudo, *Appl. Phys. Lett.* **69**, 363 (1996).

[8] *Transition Metal Oxides*, Eds. C.N.R. Rao, B. Raveau, VCH Publ., New York 1995.

[9] J. Lee, H. Shin, H. Chung, Q. Zhang, F. Saito, *Mater. Trans.* **44**, 1457 (2003).

[10] V. Manivannan, P. Parhi, J.W. Kramer, *Mater. Sci.* **31**, 987 (2008).

[11] T. Ito, S. Narita, *J. Phys. Soc. Jpn.* **39**, 140 (1975).

[12] M.W. Shafer, *J. Appl. Phys.* **40**, 1601 (1969).

[13] M.P.J. Punkkinen, *Solid State Commun.* **111**, 477 (1999).

[14] P. Hohenberg, W. Kohn, *Phys. Rev. B* **136**, 864 (1964).

[15] A. Bentouaf, F.H. Hassan, *J. Magn. Magn. Mater.* **381**, 65 (2015).

[16] A. Abbassi, M. Arejdal, H. Ez-Zahraouy, A. Benyoussef, *Opt. Quant. Electron.* **48**, 38 (2016).

[17] P. Blaha, K. Schwarz, G.K.H. Madsen, *Comput. Phys. Commun.* **147**, 71 (2002).

[18] W. Kohn, L.J. Sham, *Phys. Rev.* **140**, 1133 (1965).

[19] J.P. Perdew, K. Burke, M. Ernzerhof, *Phys. Rev. Lett.* **77**, 3865 (1996).

[20] F. Tran, P. Blaha, *Phys. Rev. Lett.* **102**, 226401 (2009).

[21] F.D. Murnaghan, *Proc. Natl. Acad. Sci. USA* **30**, 244 (1944).

[22] M. Jamal, Cubic-elastic, 2012.

[23] P. Blaha, K. Schwarz, G.K.H. Madsen, D. Kvasnicka, J. Luitz, "WIEN2K, An Augmented-Plane-Wave + Local Orbitals Program for Calculating Crystal Pro-perties", Technische Universität Wien, Wien 2001.

[24] R.L. Moreira, A. Dias, *J. Phys. Chem. Solids* **68**, 1617 (2007).

[25] L.Q. Jiang, J.K. Guo, H.B. Liu, M. Zhu, X. Zhou, P. Wu, C.H. Li, *J. Phys. Chem. Solids* **67**, 153 (2006).

[26] M. Abdul, S.L. Yeon, *Adv. Inf. Sci. Serv. Sci.* **2**, 3 (2010).

[27] A.S. Verma, A. Kumar, S.R. Bhardwaj, *Phys. Status Solidi B* **245**, 1520 (2008).

[28] A.S. Verma, A. Kumar, *J. Alloys Compd.* **541**, 210 (2012).

[29] W. Travis, E.N.K. Glover, H. Bronstein, D.O. Scanlon, R.G. Palgrave, *Chemical Science*, The Royal Society of Chemistry, 2016.

[30] N. Erum, M.A. Iqbal, *Solid State Commun.* **264**, 39 (2017).

[31] M.H. Sadd, *Elasticity Theory, Applications, and Numerics*, Elsevier Academic Press, 2005.

[32] G. Pari, S. Mathi Jaya, R. Asokamani, *Phys. Rev. B* **50**, 8166 (1994).

[33] R. Ubic, *J. Am. Ceram. Soc.* **90**, 3326 (2007).

[34] Z. Ali, I. Khan, I. Ahmad, M.S. Khan, S.J. Asadabadi, *Mater. Chem. Phys.* **162**, 308 (2015).

[35] J.B. Goodenough, *Rep. Prog. Phys.* **67**, 1915 (2004).

[36] N. Xu, H. Zhao, X. Zhou, W. Wei, X. Lu, W. Ding, F. Li, *J. Hydrog. Energy* **35**, 7295 (2010).

[37] M. Kocsis, in: *1999 IEEE Nuclear Science Symp. — Conf. Record*, Vols. 1–3, IEEE, New York 1999, p. 741.

[38] N. Erum, M.A. Iqbal, *Mater. Res. Express* **5**, 025904 (2018).

[39] B. Holm, R. Ahuja, Y. Yourdshahyan, B. Johansson, B.I. Lundqvist, *Phys. Rev. B* **59**, 12777 (1999).

[40] G.T. Mase, G.E. Mase, *Elasticity: Theory, Applications, and Numerics*, 2nd ed., CRC Press LLC, 1999.

[41] A. Meziani, H. Belkhir, *Comput. Mater. Sci.* **61**, 67 (2012).

[42] G. Hautier, C. Fischer, V. Ehrlacher, A. Jain, G. Ceder, *Inorg. Chem.* **50**, 656 (2011).

[43] S. Sugano, Y. Tanabe, H. Kamimura, *Multiplets of Transition-Metal Ions in Crystals*, Vol. 70, 1st ed., Academic Press, New York 1970.

[44] A. Meziani, D. Heciri, H. Belkhir, *Physica B* **406**, 3646 (2011).

[45] P.W. Anderson, H. Hasegaw, *Phys. Rev.* **100**, 675 (1955).

[46] M. Harmel, H. Khachai, M. Ameri et al., *Int. J. Mod. Phys. B* **26**, 1250199 (2012).

[47] R. Hill, *Proc. Phys. Soc. Lond. A* **65**, 349 (1952).

[48] A. Reuss, *Z. Angew. Math. Phys.* **9**, 49 (1929).

[49] W. Voigt, *Ann. Phys.* **38**, 573 (1889).

[50] S.F. Pugh, *Philos. Mag.* **45**, 823 (1954).

[51] M.G. Brik, *J. Phys. Chem. Solids* **71**, 1435 (2010).

[52] D.G. Pettifor, *Mater. Sci. Technol.* **8**, 345 (1992).

[53] J. Callaway, *Quantum Theory of the Solid State*, 2nd ed., Academic Press, New York 1991.

[54] A.A. Mubarak, S. Al-Omari, *J. Magn. Magn. Mater.* **382**, 211 (2015).

[55] O.L. Anderson, *J. Phys. Chem. Solids* **24**, 909 (1963).

[56] M. de Jong, W. Chen, T. Angsten, et al., *Sci. Data* **2**, 150009 (2015).

[57] J.-P. Poirier, *Introduction to the Physics of the Earth's Interior*, 2nd ed., Cambridge University Press, United Kingdom 2008, p. 131.

[58] T.M. Holden, W.J.L. Buyers, E.C. Svensson, R.A. Cowley, M.T. Hutchings, D. Hukin, R.W.H. Stevenson, *J. Phys. C Solid State Phys.* **4**, 2127 (1971).

[59] I. Sakho, A.S. Ndao, M. Biaye, A. Wague, *Phys. Scr.* **74**, 180 (2006).

[60] C. Zener, *Phys. Rev.* **82**, 403 (1951).

[61] R. Hoffman, *Rev. Mod. Phys.* **60**, 801 (1988).

[62] S. Blundell, *Magnetism in Condensed Matter*, Oxford University Press, New York 2001.

[63] D.J. Mackin, R.L. Martin, R.S. Nyholm, *J. Chem. Soc.*, 1490 (1963).

[64] R.H. Langley, C.K. Schmitz, M.B. Langley, *J. Chem. Educ.* **61**, 643 (1984).

[65] J.C. Slater, *Phys. Rev.* **49**, 537 (1936).

[66] M. Fox, *Optical Properties of Solids*, Oxford University Press, New York 2001.

[67] S. Kumar, T.K. Maury, S. Auluck, *J. Phys. Condens. Matter* **20**, 075205 (2008).

[68] G. Zanmarchi, P.F. Bongers, *Solid State Commun.* **6**, 27 (1968).

[69] M.J. Weber, *Handbook of Optical Materials*, CRC Press LLC, 2003.